INSTITUTE OF PHYSICS PUBLISHING JOURNAL OF MICROMECHANICS AND MICROENGINEERING
J. Micromech. Microeng. **11** (2001) 672–685 PII: S0960-1317(01)24094-7

Sub-micrometer solid-state adhesive bonding with aromatic thermosetting copolyesters for the assembly of polyimide membranes in silicon-based devices

J C Selby[1], M A Shannon[1], K Xu[2] and J Economy[2]

[1] Department of Mechanical and Industrial Engineering, University of Illinois at Urbana-Champaign, 1206 W Green Street, Urbana, IL 61801, USA
[2] Department of Materials Science and Engineering, University of Illinois at Urbana-Champaign, 1304 W Green Street, Urbana, IL 61801, USA

Received 19 April 2001, in final form 17 September 2001
Published 12 October 2001
Online at stacks.iop.org/JMM/11/672

Abstract
An adhesive bonding process is presented that utilizes sub-micrometer thick bondlines of all-aromatic thermosetting copolyesters (ATSP) for the assembly of polyimide membranes in silicon-based sensors and actuators. Due to the unique ability of ATSP to form void-free self-adhesive bonds through solid-state interchain transesterification reactions, sub-micrometer adhesive bonding technology offers new avenues for the precision assembly of high-performance, three-dimensional microscopic and mesoscopic devices. As a model process, PMDA-ODA polyimide membranes, 4–6 μm thick, are fabricated on glass carrier substrates, selectively bonded, transferred, and assembled on bulk-micromachined silicon substrates in the fabrication of mesoscopic circular diaphragm structures, 2–8 mm in diameter. Experimental load–deflection behavior of adhesively bonded polyimide diaphragms demonstrate that assembled membranes exhibit a tensile residual stress of 19 MPa, a value roughly equal to that measured for a PMDA-ODA polyimide film (derived from a thermally imidized polyamic acid precursor) deposited directly on silicon. Using a standard blister-type peel test, the debond energy range of an assembled polyimide membrane is shown to be 15–23 J m^{-2}, approximately 15–25% of the debond energy measured for a PMDA-ODA polyimide film deposited directly on a silicon substrate with a native oxide surface.

(Some figures in this article are in colour only in the electronic version)

1. Introduction

Devices that integrate sensors and actuators with critical dimensions that span the microscale to the normal scale (1 μm < length scale < 1 cm) have recently garnered much attention from the microengineering community. Fabrication of these devices (often referred to as mesoscopic devices), such as chemical reactors, synthesizers, heat pumps, fuel cells, combustors and refrigeration systems [1, 2], is not easily accessible using standard microfabrication technologies alone. Robust manufacture draws upon both traditional micromachining as well as the development of new fabrication technologies, such as new and improved assembly and bonding techniques.

Polymers are the most predominantly used adhesives in device assembly, wafer bonding, encapsulation, and packaging schemes. Typically, adhesive bonding with thermosetting or thermoplastic polymers provides the advantages of low bonding temperatures, no metal ion contamination, low thermal stresses, and moderate bond strengths between a broad range of materials. However, many polymer adhesives have low thermal stability, high vapor pressures, are difficult to

0960-1317/01/060672+14$30.00 © 2001 IOP Publishing Ltd Printed in the UK

pattern, and have severe incompatibility problems with other standard microfabrication processes [3, 4]. Various adhesive bonding techniques that use polymers for the assembly of micromachined components have been proposed for laboratory scale production of microscopic and mesoscopic devices, utilizing photoresists, polymethylmethacrylate (PMMA) [5], photosensitive polyimides (PSPI) [6, 7], and commercial epoxies [8].

The assembly of polyimide membranes in microscopic and mesoscopic devices based on pneumatic, electrostatic, or magnetic diaphragm actuation represents a specific application well suited for adhesive bonding. In general, a membrane assembly technique involves membrane fabrication on a carrier substrate, followed by bonding and transfer of the membrane from the carrier substrate to the device in a process that achieves microscopic tolerances. Epoxy-based bonding developed for the manufacture of micro-molded polymer pumps and valves offers one practical approach to the assembly of polyimide membranes [9]. As evidence, several generations of pumps and valves have been fabricated using an epoxy-based adhesive bonding process and diaphragm transfer to assemble polyimide membranes with polysulfone (PSU) and/or PMMA substrates [10–12]. The main advantages of the epoxy-based membrane assembly technique are that it is performed at low process temperatures and that it proceeds without the evolution of volatiles to corrupt the bondline. However, a few distinct disadvantages emerge when the technique is used to assemble polyimide membranes with silicon substrates to create mesoscopic diaphragms/cavities. Epoxy-based bonding requires adhesive channels, traps, or injection ports incorporated into the housing of the functional device to control fluid motion of the epoxy precursors. Although for injection-molded plastic components these structural features are a rather modest design accommodation, preparation of silicon substrates suitable for bonding would necessitate several additional, expensive bulk-micromachining processes. In addition, epoxy-based adhesive bonding techniques prove to be difficult to use when attempting to controllably bond membranes (diaphragms) that span large planar areas with sub-micrometer bondlines. Although silicon remains one of the most common substrate materials for microscopic and mesoscopic devices, fabrication issues concerning the assembly of layered polymer membranes in a stack of bulk-micromachined silicon substrates have been largely unresolved. Schwesinger *et al* [13], in work on the fabrication of a micropump for viscous liquids, concluded that "(adhesive) bonding of polymer (i.e. polyimide) materials with smooth silicon surfaces is a severe problem".

In an attempt to address the need for a polyimide membrane assembly technology for silicon-based microscopic and mesoscopic devices, this paper presents an assembly technique based on sub-micrometer solid-state adhesive bonding with a recently developed new family of all-aromatic thermosetting copolyesters (ATSP) [14]. The paper is organized as follows. Section 2 outlines the significant properties and processing of ATSP thin films, and section 3 details the unique self-adhesive bonding process of ATSP thin films made possible by interchain transesterification reactions (ITR). Section 4 presents the polyimide membrane assembly technique through the fabrication of mesoscopic circular diaphragm structures. Finally, section 5 evaluates the assembly technique, identifying the effects of the bonding process on the mechanical properties of assembled membranes as well as quantifying the adhesive strength of the ATSP/native silicon oxide interface.

2. Aromatic thermosetting copolyesters

Commercially available polymeric materials such as PMMA, polyimide (Pyralin® PI-2808, PI-2611), and epoxies (EPON® SU-8) have facilitated progress in micromachining technology. Circa 1996, Frich *et al* [15] developed a new family of ATSP that integrated many key physical properties and processing attributes of the above polymer systems into a single material. ATSP is a thermosetting polyester created by endothermic condensation reactions of low molecular weight acetoxy and carboxylic acid end-capped oligomers at elevated temperatures. Thin-film ATSP is derived from carboxylic acid end-capped oligomers, classified as C-1, with four functional groups and an average molecular weight of 6500 g mol^{-1}, as well as acetoxy end-capped oligomers, classified as A-1, with four functional groups and an average molecular weight of 7000 g mol^{-1}. One possible representation of the synthesized C-1 and A-1 oligomers and their associated cure reaction can be viewed in figure 1.

2.1. Thin-film processing

Sub-micrometer ATSP films are created on planar substrates using spin-coat deposition of C-1/A-1 oligomers, pre-bake, and partial or full thermal cure. Solutions used for spin coating are obtained by mixing purified oligomeric pre-polymer powders in a 1.1:1 weight ratio (C-1:A-1) and dissolving them in N-methyl pyrrolidinone (NMP) up to a 10 wt% concentration [14]. Once fully or partially cured, traditional photolithographic and reactive ion etching (RIE) processes can be utilized for pattern generation in ATSP films. Detailed accounts of the development of these basic processing techniques for ATSP thin films can be found elsewhere [16].

2.1.1. Deposition and pre-bake. The C-1/A-1 system is a two component pre-polymer mixture in which the oligomers exhibit very different solubility regimes in the primary solvent, NMP. Spin coating uniform thin films (<1 μm) from extremely low viscosity solutions is a nontrivial process, since standard spin times (20–30 s) at moderate to high spin rates (3000–5000 rpm) cause phase separation and precipitation of oligomers resulting in non-planar, inhomogeneous films. Specifically, spin-coat deposition of the C-1/A-1 system utilizes several step-wise accelerations in substrate rotation to quickly thin the film to the sub-micrometer regime by removing large slugs of solution. Following the acceleration bursts, a short hold at a moderate spin speed ensures large area uniformity of the film thickness. In order to completely suppress precipitation of oligomers, spin coating is carried out in an environment saturated with NMP vapor. A diagram of the process is shown in figure 2.

A pre-bake process that uses infrared (IR) radiation from a commercially available IR lamp drives the oligomer film into a frozen, glassy state. During the exposure, solvent evaporation

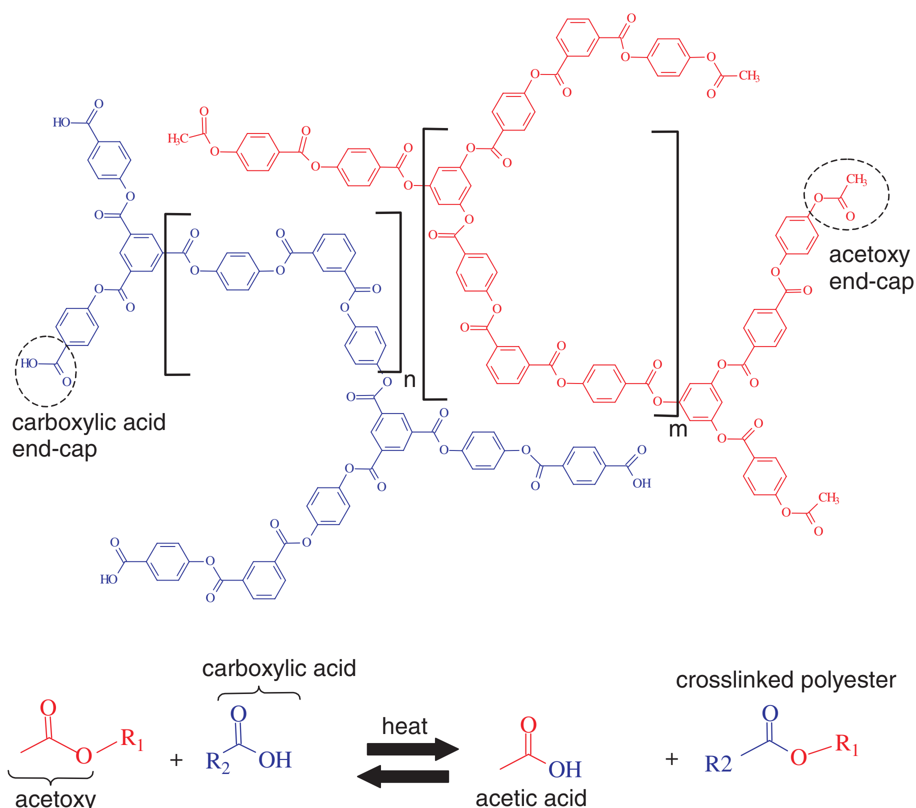

Figure 1. ATSP is formed during a condensation reaction between carboxylic acid (C-1) and acetoxy (A-1) end-capped oligomers. Acetic acid evolves as the condensation by-product.

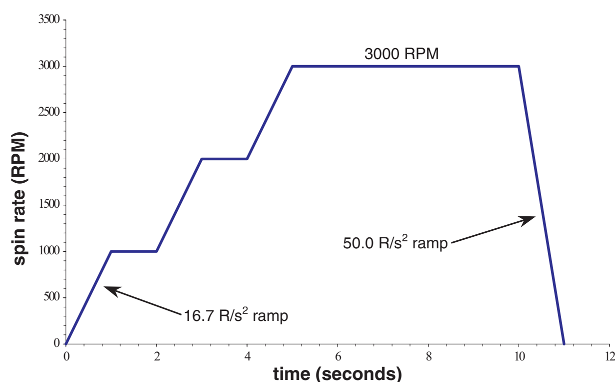

Figure 2. The diagram exhibits the spin-coating process required to deposit uniformly mixed C-1/A-1 oligomer films from 10 wt% solutions in NMP.

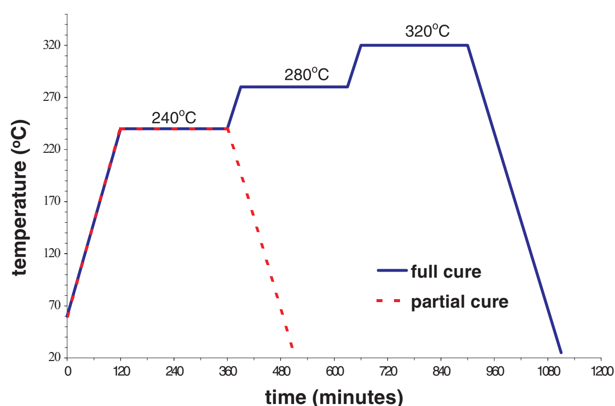

Figure 3. Partial and full cure processes performed on C-1/A-1 oligomer films spin coated from 10 wt% solutions in NMP result in 0.3 μm thick ATSP films.

is easily observed by the formation and growth of diffraction-based color rings on the surface of the substrate, culminating with the sweeping of a uniform color front across the surface of the wafer. Once the final color front has passed, no further increase in pre-bake exposure results in a macroscopically observable change of film condition. Typically, a 1–3 mm wide edge bead of increased film thickness is formed around the substrate perimeter during the pre-bake process.

2.1.2. Cure. As depicted in figure 1, curing of the C-1/A-1 oligomer system proceeds through an esterification reaction between the carboxylic acid and acetoxy end caps with acetic acid evolving as the condensation product. Past studies of curing behavior of various ATSP oligomeric precursor mixtures have primarily focused on relatively thick film (>10 μm) pre-polymer melts, which is more closely associated with bulk curing behavior [17]. The cure of a sub-micrometer C-1/A-1 oligomer film begins at a reaction temperature around 235 °C. Cures of C-1/A-1 oligomer thin films are classified as either partial or full, depending on whether or not the resultant ATSP film is to be used as a bonding layer. In various qualitative experiments, it was determined that partially cured ATSP films bonded via ITR exhibited stronger interfaces than those produced from fully cured films. A time/temperature plot of both cure schedules can be found in figure 3. All curing

was carried out in a vacuum oven with a 75 Torr pressure of dry nitrogen. Partially and fully cured ATSP films derived from oligomer films spin coated from 10 wt% solutions of C-1/A-1 have an average film thickness of 2940 ± 140 Å, or approximately 0.3 μm.

2.1.3. Pattern generation. Dry patterning of ATSP utilizes many of the same microfabrication methods previously established for other polymers. The simplest process employs an AZ® 5214 photoresist film as a physical mask, and RIE of the partially or fully cured ATSP film in an oxygen plasma. Plasma etching of ATSP proceeds at a very rapid rate (>50 Å s^{-1}). Since neither fully nor partially cured ATSP films are soluble in acetone, the photoresist mask can be removed in acetone without damaging the patterned ATSP film. A rinse of the substrate and patterned ATSP film with isopropanol completes the process.

2.2. ATSP physical properties

During the cure cycles of the C-1/A-1 oligomer films, the reaction creates an infinite three-dimensional network chain polymer, which is referred to as ATSP. No quantitative experiments have been carried out to fully characterize the mechanical or chemical properties of either partially or fully cured sub-micrometer ATSP films. However, various qualitative experiments have shown that thin-film ATSP exhibits properties that resemble those recorded for the bulk. Fully cured ATSP has degradation temperatures greater than 400 °C in inert atmospheres and around 350 °C in air. The thermal stability of ATSP, a direct consequence of an all aromatic chain structure, is comparable to that of commercially available polyimides. ATSP derived from a cured C-1/A-1 melt exhibits a high glass transition temperature (T_g) around 225 °C, a room temperature shear modulus of 1.2 GPa, and density of 1.35 g cm^{-3}. In addition to excellent solvent resistance, ATSP demonstrates very low moisture absorption of less than 0.3 wt%. Preliminary tests have revealed that fully cured ATSP possesses a thin-film breakdown strength in excess of 3×10^6 V cm^{-1} and an isotropic dielectric constant controllable down to and below 4.6.

3. Solid-state bonding via ITR

Of all the desirable properties of ATSP films derived from spin-coated solutions of C-1/A-1 oligomers, perhaps the most unique and advantageous characteristic of the material is the ability of the cured polymer network to form void-free adhesive bonds with itself through solid-state ITR.

3.1. Bond formation in polymer adhesives: thermoplastic versus thermosetting systems

For thermoplastic polymer systems, adhesive bonding processes typically consist of applying a thin film of thermoplastic material on one or both adherends, and then heating the joint to a temperature above the glass transition temperature of the thermoplastic for an appropriate time interval to allow extensive diffusion of the polymer molecules in the formation of an interfacial mechanical interlocking zone. Typically, the thermoplastic is present on both adherends prior to bonding, and the process is often referred to as polymer welding. The phenomenon has been studied by many authors [18–20], and chain entanglement is generally thought to dominate the formation and strength of an adhesive bond at the interface between two thermoplastic polymer films. Moreover, the strength of the adhesive interface formed between the thermoplastic and the adherend surface is a combination of mechanical interlocking and secondary chemical bonding, or van der Waals forces: dispersion forces, dipole–dipole interactions, and hydrogen bonds. The relative magnitudes of the chemical and mechanical contributions to the overall joint strength are often convoluted and difficult to discern.

Alternatively, adhesive bonding processes with thermosetting polymers are carried out by applying a pre-polymer material to one or both adherends, joining the adherends, and then curing the pre-polymer in the joint into a three-dimensional network or crosslinked polymer via a thermally or photochemically induced polymerization reaction. Adhesive bonds are formed as the low molecular weight pre-polymers penetrate into microporosity present on the adherend surfaces prior to crosslinking, mechanically anchoring the two substrates. Depending on adherend surface composition, the potential for primary and secondary chemical bonding at the interface between the thermoset and the adherend is also inherent to most thermosetting systems. Diffusion of polymer chains is not a mechanism by which fully cured thermosetting polymer systems can form welded interfacial adhesive bonds. A thin film of a cured thermosetting polymer *cannot* be adhesively welded to another surface (including other thermosetting thin films) by chain diffusion alone, because only small chain segments are available for localized interfacial diffusion once the system is fully crosslinked.

3.2. Molecular nature of ITR

In contrast to most thermosetting polymer systems, cured ATSP films *can* be welded in the solid state, where the formation of primary chemical bonds rather than the diffusion of chains and chain segments is responsible for the consolidation and strength of the self-adhesive bondline. Specifically, ITR, which are distinct solid-state chemical reactions that occur at high temperatures between neighboring ester groups or between an ester and an adjacent carboxylic acid group, proceed to randomize the three-dimensional chain network across the interface of ATSP films in local contact. The process is illustrated in figure 4. ITR proceed through mechanisms in which the groups before and after the reactions are identical [17]. It has been shown that a typical diffusion length or modest segmental interpenetration on the order of 300 Å results from a high-temperature bonding process between ATSP films [17, 21], but this diffusion of chain segments is not responsible for the strength of the adhesive bondline. Frich *et al* [22] were the first to demonstrate solid-state adhesive bonding by ITR between fully cured ATSP thick films (100–300 μm) in the joining of titanium structural members. The process consisted of coating the adherends with oligomer C-1/A-1 melts, followed by a full thermal cure of the oligomers into ATSP films. The adherends were then aligned and bonded by ITR (without the evolution of volatiles) in a

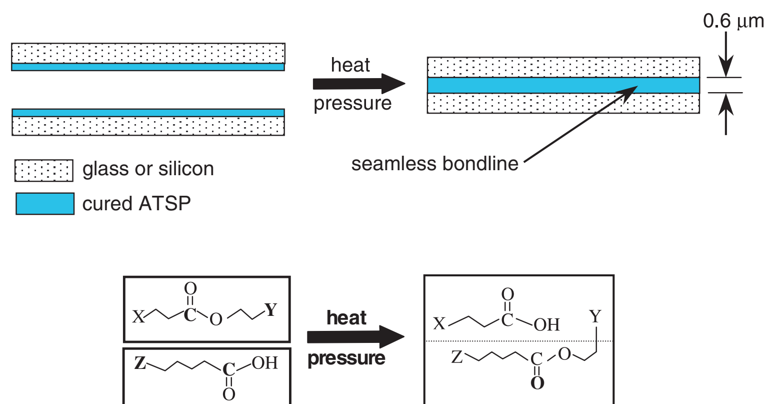

Figure 4. Sub-micrometer solid-state adhesive bonding with ATSP can be used to join two adherends coated with ATSP thin films through interfacial ITR. At a molecular level, the figure depicts ITR occurring between a carboxylic acid end group and an adjacent ester linkage, where the polyester chain segment labeled Y has in effect detached from the X chain and linked with the Z chain across the adherend interface.

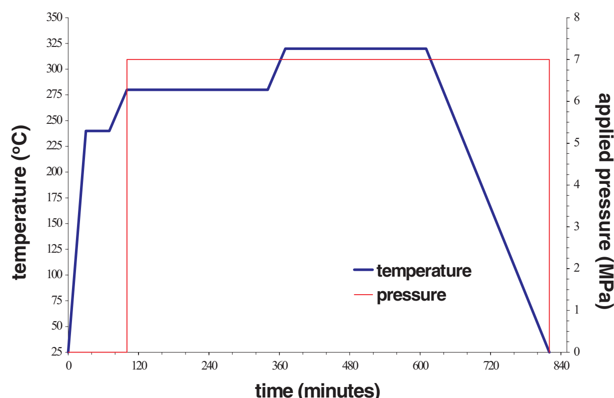

Figure 5. Elevated temperatures and pressures of the sub-micrometer solid-state ATSP adhesive bonding process prompt extensive interfacial ITR between ATSP thin films, resulting in a consolidated bondline.

vacuum hot press at 320 °C with a 1–7 MPa applied load. Lap shear strengths ranging from 15–17 MPa were observed for joints processed in this fashion.

3.3. Sub-micrometer adhesive bonding with ATSP

A technique for adhesive bonding with sub-micrometer films of ATSP was developed for inclusion in the polyimide membrane assembly process presented in section 4. The basic process for joining two planar substrates begins with the deposition, pre-bake, and partial cure of ATSP thin films on each respective substrate surface. Using an Electronic Visions Inc. 501S bonding station, the two substrates to be bonded are rapidly heated under vacuum (0.075 mTorr) at a rate of approximately 7 °C min^{-1} from 25 °C to a temperature of 240 °C, followed by a hold at 240 °C for 25 min in order to drive-off residual moisture. After the hold, samples are manually aligned and sealed with forceps at 240 °C and ambient pressure. During bonding experiments in which an optically transparent substrate was joined to an opaque substrate (glass/silicon samples), initial sealing was readily observed as the substrates zipped closed upon contact, evidence of spontaneous crack healing between the ATSP films. After sealing, vacuum conditions are imposed and the bond cycle is initiated, consisting of a continuation and completion of the full cure of C-1/A-1 oligomer films as outlined in section 2.1.2. A load ranging from 1–7 MPa is applied to the sample stacks throughout the bonding process. A time/temperature/applied load history of the process is detailed in figure 5. It is important to reiterate that in order to utilize sub-micrometer solid-state adhesive bonding with ATSP, a thin film of the cured polyester must be present on both adherends. To date, large area (>2.5 cm^2) bonding with thin-film ATSP has been limited to the use of polished silicon and glass substrates, because a spin-coated oligomer film can planarize only over surface contour variations much less than its optimal planar thickness of 0.3 μm. Scrupulously clean surfaces are also critical to bonding large areas, since any particulate present on the surface of a cured ATSP film that is larger than roughly 0.6 μm in diameter prevents intimate contact between joined adherends, precluding bondline consolidation via ITR. Alternative methods of oligomer deposition, such as spray coating or thermal evaporation, will eventually be required for more robust bonding applications that utilize substrates with large three-dimensional contour variations.

From several qualitative experiments, it was determined that the strength of joints between substrates could be maximized if the ATSP is only cured for 4 h at 240 °C. No further investigation was performed to define the phenomenon controlling the macroscopically observed differences in strength between fully or partially cured and bonded ATSP films. It is hypothesized that more carboxylic acid and acetoxy end groups are available for ITR between ATSP films that have not reached maximum fractional end-group conversion, but are beyond the theoretical gel point of the system. Additionally, partially cured ATSP films possess a lower glass transition temperature than do fully cured films, and the corresponding increase in chain mobility insures proximity of end groups. In turn, the number of potential sites for ITR to occur is increased, which drastically enhances the observed strength of the bondline. There was some concern as to whether these unreacted groups would proceed to esterify or condense as acetic acid and remain trapped in the bondline. However, scanning electron microscopy (SEM) studies of ATSP bondlines between silicon substrates freeze-fractured

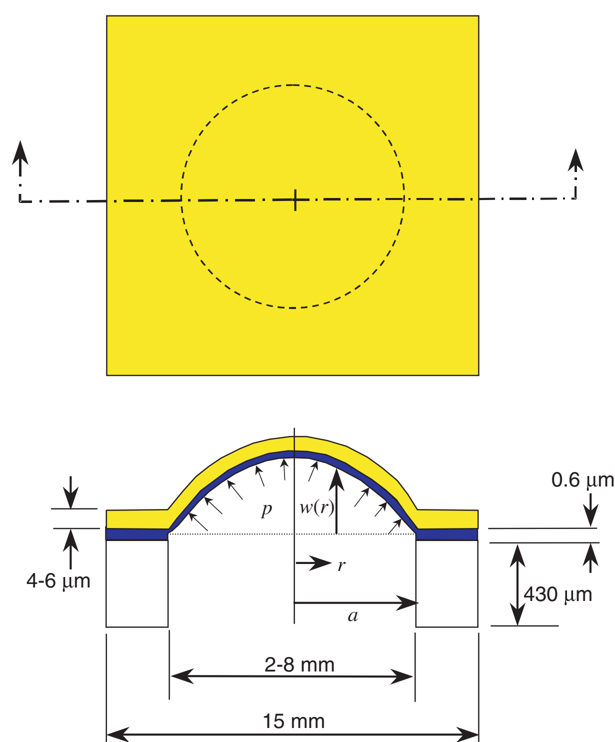

Figure 6. A mesoscopic circular diaphragm sample subject to a uniform load, p, will exhibit a deflected profile, $w(r)$.

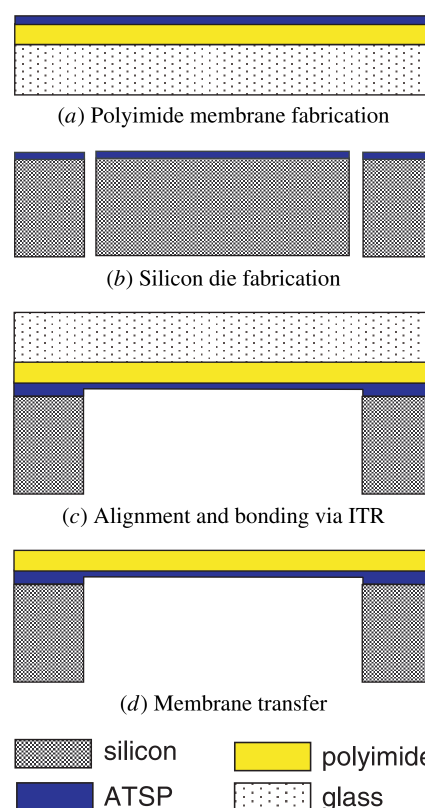

Figure 7. The fabrication process of a mesoscopic circular polyimide diaphragm structure consisting of: (*a*) fabrication, on a glass carrier substrate, of a polyimide membrane coated with a 0.3 μm thick ATSP film; (*b*) bulk-micromachining of a silicon die coated with a 0.3 μm thick ATSP film; (*c*) alignment and adhesive bonding; and (*d*) membrane transfer.

in liquid nitrogen demonstrated that solid-state adhesive bonding with partially cured ATSP films proceeds without the aggregation of volatiles and hence no large continuous voids are formed in the bondline. Additionally, these studies verified a consolidated sub-micrometer bondline thickness of approximately 0.6 μm.

4. Polyimide membrane assembly

The polyimide membrane assembly process is presented in the context of the fabrication of mesoscopic circular diaphragm structures, 2–8 mm in diameter, consisting of a 4–6 μm thick PMDA-ODA polyimide membrane assembled on a bulk-micromachined silicon substrate. Schematic representations of the mesoscopic diaphragm structure, and the fabrication sequence used for its production, can be viewed in figures 6 and 7, respectively. Sub-micrometer solid-state adhesive bonding with ATSP for the assembly of polyimide membranes requires:

(a) fabrication, on a glass carrier substrate, of a 4–6 μm thick PMDA-ODA polyimide membrane coated with a 0.3 μm thick partially cured ATSP film;
(b) bulk-micromachining of square silicon die coated with a 0.3 μm thick partially cured ATSP film;
(c) alignment and adhesive bonding of the polyimide membrane/carrier substrate to the silicon die; and
(d) transfer of the polyimide membrane from the carrier substrate to the silicon die, resulting in an assembled membrane.

Specific details of how each step is carried out in the fabrication of the mesoscopic circular diaphragm structures (figure 7) are given in the following sections.

4.1. PMDA-ODA polyimide membrane fabrication

In brief, polyimide membrane fabrication consists of a process in which Corning 7740 cover glass slides, 25 × 25 mm^2, 190–250 μm thick, are cleaned and spin coated with Pryalin® PI-2808, a PMDA-ODA polyamic acid resin from HD MicroSystems. After spinning, a 15 min pre-bake at 60 °C is performed, and the polyamic acid is then thermally imidized at 240°C for 2 h and 350 °C for 4 h, followed by an anneal back to room temperature at a rate of 1.5 °C min^{-1}. The imidization and anneal are performed under vacuum with a 200–500 mTorr pressure of dry nitrogen. Films spin coated and imidized on the cover glass substrates are 4.6±0.2 μm thick with a 2–3 mm wide perimeter edge bead. Thicknesses ranging from 4–6 μm can be achieved by varying the maximum spin rate from 2800 to 4000 rpm, respectively. The final step in membrane fabrication is to spin coat and partially cure a 0.3 μm thick ATSP film on the surface of the polyimide utilizing the process techniques detailed in sections 2.1.1 and 2.1.2. Although not previously discussed, the 10 wt% C-1/A-1 oligomer solution in NMP does not readily wet hydrophobic surfaces, such as dehydrated polyimide. Therefore, once imidization is complete, the polyimide samples are removed from vacuum and exposed to ambient temperature and humidity for at least 30 min prior to deposition of the oligomer solution. This procedure naturally conditions the polyimide films with hydrophilic surfaces more amenable to spin coating the C-1/A-1 oligomer solution.

Initially, the choice of polyimide chemistry for incorporation into the membrane assembly process was thought to be inconsequential. Previous work suggested that ATSP forms strong adhesive interfaces with BPDA-PDA polyimide (Pryalin® PI-2611) [14]. However, more refined experimentation on isolated interfaces rather than composite specimens showed that the strength of ATSP/polyimide interfaces does exhibit a dependence on polyimide chemistry. PMDA-ODA polyimide membranes transferred and assembled on silicon substrates with ATSP bondlines demonstrated strong adhesive bonds, while ATSP formed weak adhesive bonds with BPDA-PDA polyimide. From these early bond results, PMDA-ODA was selected for incorporation in the membrane assembly process, and all work with BPDA-PDA polyimide was discontinued. The working hypothesis for the observed discrepancy in polyimide/ATSP adhesion is attributed to the differences in physical chemistry or degree of molecular orientation of the imidized films. PMDA-ODA polyimide contains a flexible ether linkage within the monomer structure, whereas BPDA-PDA behaves as a rod-like molecule. Studies on the spontaneous orientation of polyimide molecules induced by thermal imidization have shown that because of this significant difference in physical chemistry, BPDA-PDA polyimides achieve a high degree of in-plane orientation during thermal imidization, while little, if any, orientation is induced in PMDA-ODA polyimides during the same process [23]. How the molecular orientation of polyimide films relates to the formation of an adhesive bond with ATSP, and moreover, the exact nature of a polyimide/ATSP adhesive interface was not investigated further within the context of microfabrication process development.

4.2. Silicon die fabrication

The fabrication scheme of the diaphragm silicon substrate consists of a wafer clean, deposition and partial cure of a 0.3 μm thick ATSP film, bulk-micromachining of die shape and through holes, and selective removal of the plasma-exposed photoresist mask. Since time multiplexed inductively coupled plasma etching, or inductively coupled plasma deep reactive ion etching (ICP-DRIE) has recently emerged as a powerful tool for the fabrication of high aspect ratios structures in silicon [24–26], it was selected for this model process in order to demonstrate how sub-micrometer solid-state adhesive bonding with ATSP can be integrated with the most recent advances in micromachining technology.

Die fabrication starts with a modified RCA clean (SC-1 only) of a 100 mm diameter, 430–440 μm thick, double-sided polished, p-doped, 1–1.5 Ω cm resistivity, n-type, $\langle 100 \rangle$ silicon wafer followed by a bake at 180 °C. The purpose of the clean process is to create a degreased silicon surface with a uniform native oxide layer, primed for subsequent deposition of an ATSP film. After the clean cycle is complete, a 10 wt% solution of C-1/A-1 oligomers in NMP is spin coated, pre-baked, and partially cured as a 0.3 μm thick ATSP film on one side of the wafer. Since thin-film deposition of ATSP is currently limited to spin-coating techniques on continuous, planar substrates, it is necessary to deposit and cure the polyester on the whole wafer rather than on the individual bulk-micromachined die.

Once the ATSP film is deposited and partially cured, the wafer is ready for ICP-DRIE to define the geometry of the diaphragm substrate. Double-sided photolithography is used to pattern 6–7 μm thick AZ® 4620 photoresist films on the front and back sides of the wafer, both of which are used as physical masks for the ICP-DRIE processes. Thick AZ® 4620 photoresist films are required to prevent damage of the underlying structural silicon and ATSP film due to the extensive duration of the etching process. The photoresist films are patterned to section the wafer into 16 individual 15 × 15 mm^2 silicon die, each separated by 200 μm wide gaps for etch channels. Moreover, all die are interconnected by 100 μm wide beams so that the wafer remains a contiguous structure throughout the entirety of the etching process. On the center of each die, either a 2, 4, 6 or 8 mm outer diameter ring, 200 μm wide, is patterned so that when etched through, the solid insert will be released, thus leaving a through hole.

A Plasma-Therm Inc. SLR Series plasma processing system was used for all ICP-DRIE processes, with RF1 and RF2 operating at 13.56 MHz and 2.0 MHz, respectively. Following a brief oxygen plasma etch (ICP-RIE) of the ATSP film to expose the native silicon surface, the wafer was etched in a modified Bosch process [25]. The oversized etch channel width of 200 μm negated any potential aspect-ratio dependent etching phenomena that might prevent efficient and complete through-etching of the wafer [26]. Combined 250 loops of the ICP-DRIE process on the back side of the wafer and 300 loops from the front side are utilized in die production. Etching from both sides of the wafer minimizes the exposure of the photoresist mask to the plasma as well as the overall process time. Once the ICP-DRIE process is complete, the sample is removed from the chamber and each individual die is separated from the wafer by snapping the connecting beams with a razor blade.

Next, the plasma-exposed photoresist film on each individual die is removed without degrading the underlying ATSP film required for bonding. In a batch process, several bulk-micromachined die are immersed in an undiluted, room temperature commercial AZ® 400K developer consisting of a solution of potassium borate and deionized (DI) water. While soaking in the developer, the die are subjected to ultrasonic agitation for 15 min. In separate experiments, negligible etching or degradation was observed in 0.3 μm ATSP films continuously exposed to the AZ® 400K developer at room temperature for 15 min. After a brief DI water rinse, the die are soaked in a solution of 0.2 M hydrochloric acid (HCl) for 5 min in order to protonate any carboxylate salts formed on the surface of the ATSP film by reaction with the developer. A final DI water rinse and nitrogen blow-dry of each individual die completes the process. Pictures of the finished die can be viewed in figure 8.

4.3. Alignment and adhesive bonding

Using an EV 501S bonding station, an ATSP/polyimide/glass membrane sample and an ATSP/silicon die are heated to 240 °C under vacuum (0.075 mTorr) and held at 240 °C for 25 min as a vacuum dehydration bake. After venting the chamber to ambient pressure, the polyimide membrane is aligned such that the planar 15 × 15 mm^2 central area of the membrane is

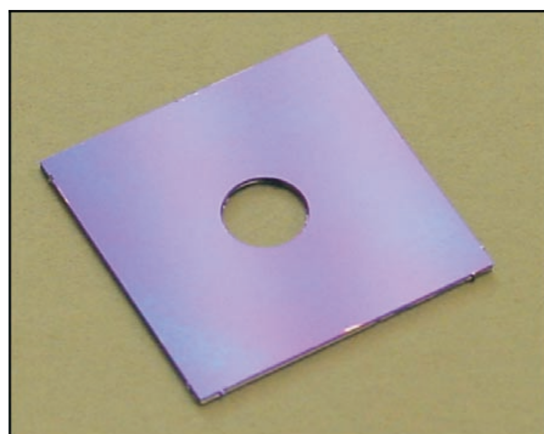

(*a*)

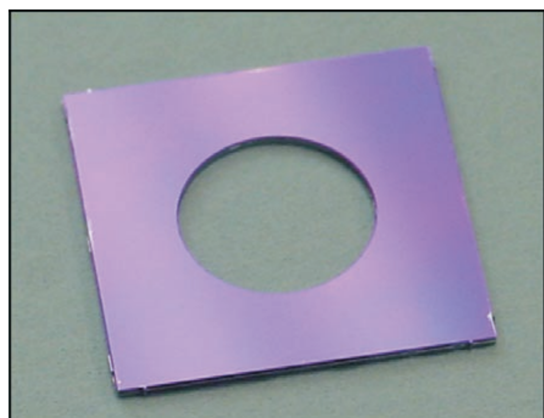

(*b*)

Figure 8. The pictures depict bulk-micromachined silicon die coated with a 0.3 μm thick ATSP film, with either (*a*) 4 mm diameter or (*b*) 8 mm diameter holes.

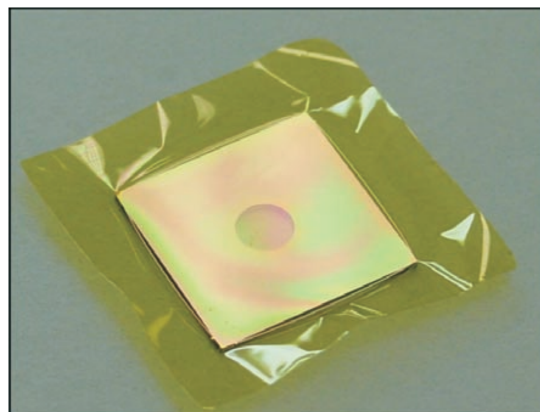

(*a*)

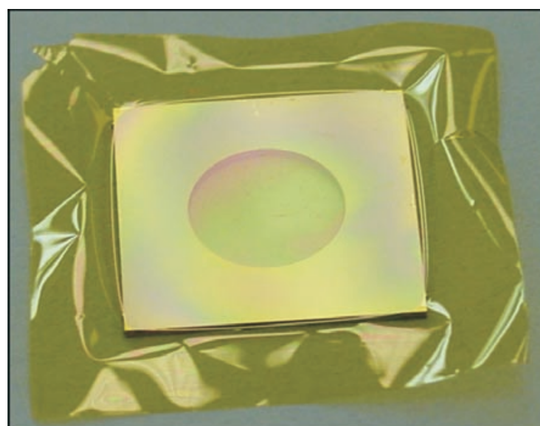

(*b*)

Figure 9. The pictures represent examples of (*a*) 4 mm diameter and (*b*) 8 mm diameter polyimide diaphragm structures fabricated by polyimide membrane assembly.

positioned at the center of the silicon die to avoid any edge bead effects. After applying a point force with the tip of a pair of stainless-steel forceps, the bondline zips along the interface of the two ATSP films in contact. The bond cycle outlined in section 3.3 is then initiated such that elevated temperatures (>280 °C) and applied pressures (1–7 MPa) result in consolidation of the bondline by ITR.

4.4. Membrane transfer

The overall process concludes with the release of the polyimide membrane from the cover glass carrier substrate to leave a circular polyimide diaphragm structure. No manipulation or manual sample handling procedure is required to release the carrier substrate. Rather, the transfer process exploits two critical material interface properties: the poor moisture resistance of a polyimide/glass (silicon oxide) interface and the excellent moisture resistance of an ATSP/silicon oxide interface. The transfer or carrier substrate release process consists of soaking the bonded stacks in DI water at a temperature of 80–90 °C for a time period of 3–4 h. During the soak, water diffuses and wicks by capillary forces in a front along the polyimide/glass interface, degrading the adhesion as it propagates. Once the water fronts from all four sides of the sample coalesce, the polyimide/ATSP/silicon stack lifts off the cover glass. The hot water process had no apparent effect on the ATSP adhesive bonds established between the polyimide membrane or the silicon die. Because polyimide absorbs water, a vacuum dehydration bake at 240 °C is performed on the released diaphragm structure. Pictures of the assembled 4 mm and 8 mm diaphragm structures can be viewed in figure 9.

5. Evaluation of assembled membranes

The PMDA-ODA polyimide membrane assembly process detailed in section 4 provides a sub-micrometer solid-state adhesive bonding technique for the fabrication of silicon-based microscopic and mesoscopic sensors and actuators. In order to demonstrate the potential utility of the technology for incorporation into future device production, several fundamental engineering properties need to be established.

5.1. Nature of ATSP/polyimide and ATSP/silicon oxide interfaces

An exhaustive study of the exact physical nature of the adhesive interfaces formed between ATSP and either PMDA-ODA polyimide or silicon oxide was not included in the development of this processing-based work. However, much information concerning the nature of these interfaces, garnered

through simple qualitative experiments, provides a basis for further enhancement of the overall joint strength through a more biased selection of processing parameters. Manual peel tests of PMDA-ODA polyimide membranes bonded to silicon substrates with sub-micrometer ATSP bondlines conclusively demonstrate that adhesive failure always occurs at the interface between ATSP and the native silicon oxide (ATSP/silicon oxide). Adhesive bonds at this interface are thought to be established during the partial cure of the C-1/A-1 oligomer film. Since C-1/A-1 oligomers possess relatively small molecular weights (but larger weights than epoxy-based precursors), some degree of mechanical interlocking between oligomer chains and the silicon oxide surface is expected. Because the silicon oxide surface is extremely smooth ($R_a < 90$ Å), little, if any, appreciable adhesion enhancement can be attributed to mechanical interlocking. Van der Waals potential interactions between the hydroxide groups of the native silicon oxide and either the acetoxy or carboxylic acid end groups of the ATSP film are thought to dominate the strength of the ATSP/silicon oxide interface.

It was surprising to discover that the adhesive interface formed between ATSP and PMDA-ODA polyimide (ATSP/polyimide) is stronger than that between ATSP and silicon oxide. As a first inclination, chemical bonds were considered as the source of adhesion since amine groups of the polyimides and ester linkages of the ATSP could interact through amine–ester interchange reactions. Since amine groups are only present as end groups of polyimide chains, their number density is exceptionally low, and thus the excellent adhesion between ATSP and PMDA-ODA polyimide cannot be conclusively attributed to these chemical interactions. Interdiffusion of entire macromolecules across interfaces in the formation of adhesive bonds is an unlikely phenomenon for arbitrary blends of long chain polymers with different chemical functionality. However, diffusion of chain segments between incompatible polymers is known to readily occur in order to minimize interfacial free energy. The ATSP thin film formed on the polyimide membrane is spin coated from solutions of C-1/A-1 oligomeric precursors dissolved in NMP, a solvent which can promote the swelling of polyimides. During the ensuing cure process of these small molecular weight oligomers, the combination of high temperatures and solvent-induced swelling of the polyimide chains can allow for substantial thermodynamically favored diffusion and interlocking of the oligomer and polyimide chains prior to completion of the fully-cured thermoset network structure of ATSP. More definitive evidence in support of this argument requires the use of neutron reflection techniques using deuterated and undeuterated thin films of ATSP.

5.2. Blister test

The most important property of any adhesive system is the strength of the resultant bond. A wide variety of adhesion tests have been developed to measure the strength of adhesives, and many of these methods are mechanically destructive. Peeling, cleavage, tensile, and lap shear tests are a few such mechanical testing methods. With regards to microfabricated thin films, one of the most widely used methods of assessing debond energy is the so-called blister test [27, 28], and therefore it was selected to quantify the debond energy of the ATSP/silicon oxide interface. By controllably loading an adhesive interface of a blister specimen until peel occurs, the failure load can be related to an ideal work of adhesion, or a non-ideal debond energy, γ_a, the latter incorporating the effects of plasticity and viscoelasticity [27].

5.3. Membrane load–deflection behavior

Determining the mechanics of deformation, or load–deflection behavior, of a suspended circular thin film is the first step towards the theoretical calculation of a debond energy, γ_a, derived from blister test experiments. Much theoretical work has been developed to model large deflections of plates and membranes of a variety of geometrical shapes, where plate analysis incorporates resistance due to bending, and membrane analysis neglects this energy in the limit as the film thickness becomes much smaller than other sample dimensions. Although more exact solutions to the mechanics of deformation of a clamped circular membrane exist [29], the analysis of Saif *et al* [30], modified to account for the presence of a uniform residual stress, was selected as the basis for load–deflection modeling.

We consider the circular membrane blister sample and its diametral cross section given in figure 6 subject to a net uniform pressure, p, resulting in the analytical deflected shape, $w(r)$. We assume that the membrane material is isotropic, behaves linear elastically, and possesses a uniform residual stress, σ_0. Only radial and tangential stresses and strains need to be considered to fully describe the load–deflection behavior. Furthermore, because the thickness of the membrane, t, is assumed to be several orders of magnitude smaller than the radius, a, bending stresses are ignored and only in-plane stresses are considered, provided they are uniform across the thickness of the membrane. Accordingly, *if the tangential strain of the membrane is assumed to be negligible*, it can be shown [16, 31] that the analytical shape, $w(r)$, of a uniformly loaded, circular diaphragm (membrane) is given by

$$w(r) = \omega_0 \left(1 - \frac{r^2}{a^2}\right) \tag{1}$$

where ω_0, the maximum central blister deflection, is implicitly evaluated from the load–deflection relation

$$p = \frac{8}{3} \frac{Et}{a^4(1-\nu^2)} \omega_0^3 + \frac{4\sigma_0 t}{a^2} \omega_0. \tag{2}$$

E and ν are Young's modulus and Poisson's ratio of the membrane, respectively. The often-cited Beams equation [32] for the load–deflection behavior of a clamped circular membrane is identical to the result expressed in equation (2) except for a missing factor of $(1 + \nu)$ in the numerator of the cubic term. Using a least-squares regression, experimentally measured load–deflection data (ω_0, p) can be fitted to a polynomial of the form of equation (2) from which the values of E and σ_0 can be extracted assuming a value of ν.

Several circular diaphragm structures, created by a polyimide membrane assembly using sub-micrometer solid-state adhesive bonding with ATSP, were fabricated as outlined in section 4 for load–deflection experiments. Specifically, the experimental diaphragms were 4, 6 or 8 mm in diameter, and

Table 1. Mechanical properties of assembled membranes.

Diameter (mm)	E (GPa)	σ_0 (MPa)
4	3.92	18.7
4	2.50	23.9
6	2.75	17.7
6	3.20	17.4
8	2.72	11.2
8	2.95	22.2

4.9 ± 0.2 μm in total thickness. It is important to note that the diaphragms were not a homogeneous membrane of PMDA-ODA polyimide, but rather a composite of a 4.6 μm polyimide layer and a 0.3 μm ATSP film. All diaphragm structures, processed in the same batch, were left exposed to ambient temperature and humidity (15–25 °C and 50–80% relative humidity) prior to load–deflection experiments to simulate typical service conditions. Once fabricated, the samples were attached, at the center, to steel test chucks using a commercially available mounting wax.

An experimental apparatus consisting of a steel cylinder with an internal piston driven by a linear piezo actuator was used for manually-controlled displacement of hydraulic oil to produce uniform applied loads on a single attached blister specimen. An Omega® PX951-100S5V pressure transducer was attached to the chamber to measure the resultant pressures, and a LMI Selcom Inc. LDS 80/10 laser distance sensor was mounted vertically above the sample to measure the corresponding maximum central blister deflections. Surprisingly, the surface of the polyimide membrane was too specularly reflective, or non-diffuse, and thus the laser was found to produce erroneous deflection measurements. To compensate, a 1 × 1 mm^2 stack of brown paper, less than 2 mm thick, was positioned at the center of the membrane, and fixed to the location using a small drop of hydraulic oil. Since the paper was not rigidly attached to the membrane, its effect was negligible on the actual membrane residual stress and modulus. The paper surface, which translated with the deflecting membrane, served as an adequate reflector for measurements with the desired 10 μm resolution of the laser. Assuming the hydraulic oil to be incompressible and if the chamber was filled properly, i.e. no trapped air bubbles, then the volumetric displacement of the oil created by translation of the internal piston would result in an identical volume generation in the deflecting blister. This type of loading of blister membranes is referred to as a constant-volume loading, or a fixed-grip condition.

Once the setup was complete, a series of load–deflection measurements were then performed by slowly incrementing the voltage supplied to the piezo, which in turn resulted in step-wise pressure increases and corresponding membrane deflections. Deflections were recorded as the membranes were both loaded and unloaded. No permanent macroscopic plastic deformation was observed during experimentation, as all deflected membranes returned to a planar, undeformed state upon unloading. A plot of typical membrane deflection behavior of 4, 6 and 8 mm diameter membranes can be viewed in figure 10. After curve fitting, the combined loading and unloading data for each individual diaphragm using the software Mathematica, Young's modulus and residual stress

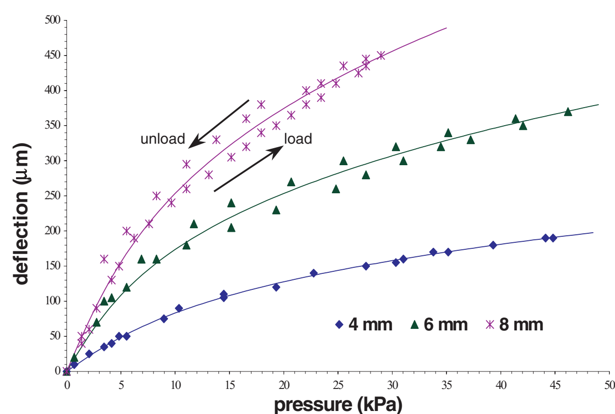

Figure 10. The plot displays measured deflections of uniformly loaded diaphragm structures. The solid curves represent least-squares curves fitted to the data for each individual diaphragm sample.

were calculated, assuming a Poisson's ratio for the membrane of 0.4 [33]. The results of these calculations can be found in table 1.

The average tensile modulus for all samples was calculated as 3.0 GPa with a standard deviation of 0.5 GPa. Over the range of values generated from samples of different diameters, all calculated mechanical properties of adhesively bonded polyimide membranes agreed to within less than a 30% difference from the average. Note that for the 6 and 8 mm diameter samples depicted in figure 10, the combined loading/unloading data clearly fall on two sides of the best-fit line for the load–deflection behavior. Deflections measured while unloading the membrane were, in general, higher than for the same applied pressure measured during the initial loading, hinting at a rate dependent, viscoelastic, stretching of the membranes.

HD MicroSystems has established a Young's modulus of 2.3 GPa for spin-coated PI-2808 PMDA-ODA polyimide films of similar thickness. However, the adhesively bonded films measured in this study are actually a composite of an ATSP thin film and a PMDA-ODA polyimide membrane. Although not readily known, ATSP is thought to possess a bulk Young's modulus of roughly 3–5 GPa. Consequently, the modulus of the ATSP/polyimide composite membrane is expected to be slightly higher than that of a homogeneous polyimide membrane. Furthermore, a deficiency of the experimental setup was that the silicon substrate was also subject to a non-uniform load during testing of the membrane. Thus, the measured membrane deflections were actually a sum of the substrate deflection plus the actual membrane deflection, altering the subsequently calculated modulus.

The average residual stress for adhesively bonded membranes was calculated as 18.5 MPa with a standard deviation of 4.4 MPa. PMDA-ODA polyimide films directly coated on silicon oxide surfaces using standard microfabrication processing techniques have been shown to have an average residual stress of 20.6 MPa [27]. It is well known that the residual stress of a micromachined polymer thin film can be affected not only by the deposition method, but also by the subsequent processing steps and environmental conditions, i.e. thermal cycling and solvent exposure, to which

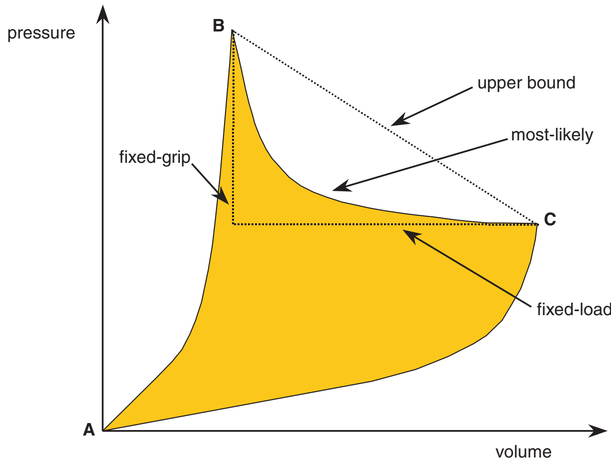

Figure 11. A schematic P–V diagram of a typical blister peel cycle under quasi-fixed-grip loading conditions. The solid line represents the most-likely P–V path followed during peel. Fixed-load and fixed-grip paths are indicated as dashed lines.

the film is subjected during device fabrication. Any deviations in the fabrication of an adhesively bonded membrane from the specific processing steps detailed in section 4 can and will affect the observed residual stress of the membrane.

5.4. Adhesive fracture

The work of Allen and Senturia [28] was chosen as the basis for the adhesive fracture model to quantify the adhesive strength of the Si/ATSP interface. Specifically, their work accounts for the presence of residual stresses in the analytical calculation of debond energy for a circular blister specimen with a fixed-grip loading condition. Neglecting the effects of plastic deformation occurring during adhesive fracture, it can be shown that the debond energy, γ_a, of a clamped, circular membrane of radius, a, measured for a blister peeled under fixed-grip loading conditions is given by

$$\gamma_a = \frac{5}{3}\frac{Et}{(1-\nu^2)}\frac{\omega_0^4}{a^4} + 2\sigma_0 t\frac{\omega_0^2}{a^2} \tag{3}$$

where ω_0 is the peak deflection at which peel ensues [16]. Equation (3) is derived by assuming the load–deflection behavior given in equation (2), and following the same energy method of linear elastic fracture mechanics applied by Allen [28]. By combining equations (2) and (3), the debond energy of a blister of a known radius can be related to the critical pressure, p_{critical}, and peak deflection, ω_0, at which crack propagation is first observed

$$\gamma_a = \frac{5}{8}p_{\text{critical}}\omega_0 - \frac{1}{2}\sigma_0 t\frac{\omega_0^2}{a^2}. \tag{4}$$

An alternative experimental method of calculating the debond energy from the quasi-fixed-grip blister test apparatus described in section 5.3 can be carried out with a pressure–volume (P–V) analysis. We consider the P–V plot of a peel cycle given in figure 11. As incremental voltages are supplied to the piezo translator, a blister of radius a_1, will deflect according to its elastic load–deflection behavior along the path from point A to point B. Using the laser sensor, the maximum central deflection, ω_0, can be measured for each applied pressure, which can then be matched to a blister volume, Δ, or

$$\Delta = \tfrac{\pi}{2}a^2\omega_0 \tag{5}$$

where a is the radius of the blister. Once the critical pressure has been reached at point B, the voltage supplied to the piezo is held constant, and the blister will begin to peel along a path from point B to point C. Peeling does not occur at a constant volume because of the finite stiffness, or compliance of the piezo translator, and thus the experiment is not a true model of constant-volume or fixed-grip adhesive fracture. Rather, adhesive fracture occurs under mixed loading conditions. As peel ensues and the pressure of the system decreases, the piezo translator will relax in proportion to pressure changes, forcing additional volumes of the incompressible hydraulic oil into the blister. During peel, measured deflections cannot be matched to a blister volume because the radius is changing, and thus the exact P–V path followed from point B to point C is not known. The most likely peel path is indicated by the solid curve in figure 11. To obtain a lower bound on the experimentally measured debond energy, the path from point B to point C, decomposed into fixed-grip and fixed-load lines, is assumed. Alternatively, to obtain an upper bound for the debond energy, the peel path is constrained to follow an approximately linear P–V path from point B to point C. The P–V peel paths that fall above this upper bound are not physically possible since they would require additional energy, or in this case increasing the voltage applied to the piezo during the peel process. Finally, after peeling is terminated at point C, the voltage supplied to the piezo is incrementally decreased, and the blister is unloaded along the path from point C to its undeformed state at point A. The blister pressures and central deflections can be measured, and the corresponding volumes associated with unloading can be calculated with equation (5) using the new blister radius, a_2. Neglecting all thermal losses and inelastic deformations, the shaded region contained within the peel cycle reflects the dissipated energy of the system, or the debond energy, γ_a, multiplied by the total area peeled, or $\pi(a_2^2 - a_1^2)$.

All fracture experiments were carried out on the apparatus described in section 5.3. Due to difficulties in achieving pressures that would induce adhesive fracture, 8 mm diameter samples could not be used, and thus only 4 and 6 mm diameter diaphragm samples were utilized. By slowly incrementing the voltage supplied to the piezo, each blister sample was loaded in the elastic load–deflection regime, continuously recording data in real time to monitor the pressure increases corresponding to piezo displacement. Once the critical pressure, p_{critical}, for the given blister of radius, a_1, has been surpassed, crack propagation occurs and the blister peels concentrically. At this point, the voltage applied to the piezo was left undisturbed. Peeling terminated once the pressure of the system fell below the critical pressure for the new radius of the blister, a_2, or a new equilibrium state of the system. Blisters did not grow catastrophically because of the quasi-fixed-grip, rather than purely fixed-load, experimental loading condition. Following crack propagation, the blister was then returned to the undeformed state by stepping back the internal piston, or reducing the voltage supplied to the piezo, and recording the corresponding pressures and central deflections. Using the laser beam as an indicator, the new

Table 2. Debond energy of ATSP from silicon oxide.

Initial blister diameter (mm)	Final blister diameter (mm)	γ_a: equation (4) (J m^{-2})	γ_a: lower bound (J m^{-2})	γ_a: upper bound (J m^{-2})
4	9.6	19.4	21.2	32.0
4	N/A[a]	10.8	N/A[a]	N/A[a]
6	10.7	12.5	11.0	14.6
6	9.3	17.9	21.0	23.4

[a] Failures in data acquisition prevented creation of a P–V plot for integration.

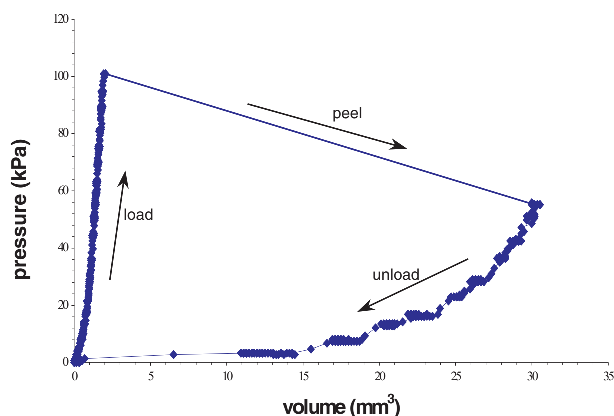

Figure 12. The plot exhibits the experimentally measured, upper bound P–V peel cycle of a blister (diaphragm) sample with a 4 mm initial diameter and a 9.6 mm peeled diameter. The critical pressure was measured at 100 kPa corresponding to a maximum deflection of 330 μm.

blister radius was measured *in situ*, to an estimated accuracy of ±5%. Table 2 contains the values for debond energy of ATSP from a native silicon oxide calculated using the analytical fixed-grip model, or equation (4), as well as upper and lower bounds of debond energy directly measured by integrating the P–V paths followed during the blister peel cycle. A plot of a typical P–V peel cycle (upper bound) of a 4 mm diameter membrane can be viewed in figure 12.

The average value of debond energy of ATSP from native silicon oxide calculated using equation (4) was found to be 15.2 J m^{-2}. All debond energies calculated for the 4 and 6 mm diameter samples agreed to within less than a 30% difference from the average. Because the experimental apparatus did not exhibit a true fixed-grip loading condition, the values generated by equation (4) are not an absolute measure of debond energy, but rather provide only semi-quantitative information. Debond energies ascertained by integration of the P–V peel cycle performed on 4 and 6 mm diameter samples had an average lower bound value of 17.7 J m^{-2} and an average upper bound value of 23.3 J m^{-2}. Integration of P–V work for the measurement of a debond energy provides the only absolute quantification of the adhesive strength of the system. Deviations in the measured debond energies are attributed to experimental deficiencies, namely the inevitable presence of trapped gases in the oil contained in the chamber, and pressure loss through cracks in the blister sample/wax interface incurred during the mounting procedure.

As a reference value, a debond energy of 93 J m^{-2} ± 15% has been experimentally measured for a PMDA-ODA polyimide film, 2.5 μm thick, coated on a silicon oxide surface in the presence of an aminosilane adhesion promoter [27]. Thus, the debond energy of a membrane adhesively bonded with a sub-micrometer ATSP bondline is roughly 15–25% of the value achieved using standard two-dimensional planar fabrication techniques. One might argue that the adhesion of PMDA-ODA polyimide achieved by traditional microfabrication processing is far superior to that of the adhesively bonded membrane, but such a comparison fails to recognize the fundamental difference between the two fabrication techniques. A fully-imidized PMDA-ODA polyimide film does not naturally adhere to *any* surface other than the primary substrate upon which the polyamic acid resin was originally deposited. However, sub-micrometer solid-state bonding with ATSP creates an adhesive bond between a fully-imidized polyimide film and a second substrate, *not* the primary substrate used for film deposition.

Ultimately, it is not yet known if the debond energy range of 15–23 J m^{-2} for the ATSP/silicon oxide system represents an optimized adhesive strength. Many different avenues of adhesion enhancement, i.e. wet chemical surface treatments, micro-texturing of surfaces, and chemical coupling agents, remain to be explored. Dry surface treatments such as ICP-DRIE and even more basic RIE technologies can be used to control the roughness and morphology of silicon oxide surfaces, allowing the design of micro-textures that enhance mechanical interlocking. Inevitably, the blister test experiment was used only to quantify the more fundamental mechanical properties of adhesively bonded membranes. The exact nature, or the dominant physical interactions, of adhesive bonds formed at ATSP/polyimide and ATSP/silicon oxide interfaces can only be studied by more advanced surface spectroscopic and microscopy techniques.

6. Conclusions

A new family of all-aromatic thermosetting copolyesters was found to possess many desired attributes of an ideal adhesive system for new and improved, microscopic and mesoscopic device assembly. ATSP is moisture-insensitive, chemically inert, patternable, possesses high thermal stability, demonstrates strong adhesive bonds with PMDA-ODA polyimide, and is amenable to standard micromachining processes. Most importantly, the ability of ATSP to form self-adhesive bonds through solid-state interchain transesterification reactions prompted the development of a sub-micrometer adhesive bonding and polyimide membrane assembly process. A process was presented in which 4–6 μm thick PMDA-ODA polyimide membranes were fabricated on glass carrier substrates, and then later selectively bonded, transferred, and assembled on bulk-micromachined silicon

die using sub-micrometer solid-state adhesive bonding with ATSP. Using a blister test analysis, PMDA-ODA polyimide diaphragms, 4–8 mm in diameter, fabricated by adhesive bonding and membrane assembly were found to possess roughly equal levels of residual stress compared to membranes directly coated on silicon oxide surfaces (19 MPa) and a slightly higher modulus (3.0 GPa versus 2.3 GPa). The debond energy range of ATSP/silicon oxide interfaces was found to be 15–23 J m^{-2}, roughly 15–25% of the debond energy of PMDA-ODA polyimide films directly coated on silicon with native oxides present.

A variety of bonding technologies have been successfully applied and demonstrated in the fabrication of planar, two-dimensional MEMS devices, but no single technique can meet the complex design and operational constraints of truly three-dimensional devices with critical dimensions ranging from micrometers to millimeters. From a broad perspective, the ability to fabricate polyimide membranes and then adhesively bond these membranes to functional substrates with sub-micrometer adhesive bondlines will ultimately enable the production of a variety of pumps, valves, and compressors based on the pneumatic, electrostatic, or magnetic actuation of diaphragms. Arguably, advanced bonding and assembly technologies hold the key to the evolution of future generations of high-performance microscopic and mesoscopic machines.

Acknowledgments

The authors would like to thank Huseyin Sehitoglu, Taher Saif, and Erdem Alaca for their help in the design of the blister test apparatus. This work was supported under DARPA DSO, contract No. DABT63-97-C-0069.

References

[1] Mehra A and Waitz A 1998 Development of a hydrogen combustor for a microfabricated gas turbine engine *Tech. Digest of the 1998 Solid-State Sensor and Actuator Workshop (June 1998)* pp 35–40

[2] Shannon M, Philpott M, Miller N, Bullard C, Beebe D, Jacobi A, Hrnjak P, Saif T, Aluru N, Sehitoglu H, Rockett A and Economy J 1999 Integrated mesoscopic cooler circuits (IMCCs) *Proc. ASME, Advanced Energy System Division* vol 39, pp 75–82

[3] Cohn M, Bohringer K, Noworolski J, Singh A, Keller C, Goldberg K and Howe R 1998 Microassembly technologies for MEMS *Proc. SPIE, Microfluidic Devices and Systems (September 1998)* pp 2–16

[4] Den Besten C, van Hal R E G, Munoz J and Bergveld P 1992 Polymer bonding of micromachined silicon structures *Proc. IEEE Micro Electro Mechanical Systems Workshop (February 1992)* pp 104–9

[5] Eaton W P, Risbud S H and Smith R L 1994 Silicon wafer-to-wafer bonding at $T < 200$ °C with polymethylmethacrylate *Appl. Phys. Lett.* **65** 439–41

[6] Frazier A B 1996 Low temperature IC-compatible wafer-to-wafer bonding with embedded micro channels for integrated sensing systems *Proc. IEEE 38th Midwest Symposium on Circuits and Systems (1996)* pp 505–8

[7] Glasgow I K, Beebe D J and White V E 1999 Design rules for polyimide solvent bonding *Sensors Mater.* **11** 269–78

[8] Maas D, Bustgens B, Fahrenberg J, Keller W, Ruther P, Schomburg W K and Seidel D 1996 Fabrication of microcomponents using adhesive bonding techniques *Proc. IEEE Micro Electro Mechanical Systems Workshop (February 1996)* pp 331–6

[9] Schomburg W K, Bacher W, Bier W, Bustgens B, Fahrenberg J, Goll C, Maas D, Menz W and Seidel D 1995 Fabrication of Microfluidic Devices by Thermoplastic Molding and Diaphragm Transfer *Proc. ASME, Dynamic Systems and Control Division* vol 57-2, pp 951–6

[10] Bustgens B, Bacher W, Ehnes R, Maas D, Ruprecht R and Schomburg W K 1994 Micromembrane Pump Manufactured by Molding *Proc. 4th Int. Conf. on New Actuators (June 1994)* pp 86–90

[11] Goll C, Bacher W, Bustgens B, Maas D, Menz W and Schomburg W K 1996 Microvalves with bistable buckled polymer diaphragms *J. Micromech. Microeng.* **6** 77–9

[12] Goll C, Bacher W, Bustgens B, Maas D, Ruprecht R and Schomburg W K 1997 An electrostatically actuated polymer microvalve equipped with a movable membrane electrode *J. Micromech. Microeng.* **7** 224–6

[13] Schwesinger N and Bechtel S 1998 Micropump for viscous liquids and muds *Proc. SPIE, Microfluidic Devices and Systems (September 1998)* pp 40–5

[14] Xu K, Economy J and Shannon M 2000 A General Purpose Adhesive for Microelectronic Devices *Int. J. Microcircuits Electron. Packag.* **23** 78–84

[15] Frich D, Goranov K, Schneggenburger L and Economy J 1996 Novel high-temperature aromatic copolyester thermosets: synthesis, characterization, and physical properties *Macromolecules* **29** 7734–9

[16] Selby J C 2001 Sub-micron solid-state adhesive bonding with aromatic thermosetting copolyesters for the transfer and assembly of microfabricated PMDA-ODA polyimide membranes *MSc Thesis* University of Illinois at Urbana-Champaign

[17] Frich D J 1996 The effect of interchain transesterification reactions on the development of aromatic copolyesters *PhD Thesis* Department of Materials Science and Engineering, University of Illinois at Urbana-Champaign

[18] Brochard-Wyart F 1991 Kinetics of polymer–polymer interdiffusion *Fundamentals of Adhesion* ed L-H Lee (New York: Plenum) pp 181–206

[19] Brown H R, Yang A C M, Russel T P, Volksen W and Kramer E J 1988 Diffusion and self-adhesion of the polyimide PMDA-ODA *Polymer* **29** 1807–11

[20] Wool R P 1991 Welding, tack, and green strength of polymers *Fundamentals of Adhesion* ed L-H Lee (New York: Plenum) pp 207–48

[21] Frich D, Hall A and Economy J 1998 Nature of adhesive bonding via interchain transesterification reactions (ITR) *Macromol. Chem. Phys.* **199** 913–21

[22] Frich D, Economy J and Goranov K 1997 Aromatic copolyester thermosets: high temperature adhesive properties *Polym. Eng. Sci.* **37** 541–8

[23] Hasegawa M, Okuda K, Horimoto M, Shindo Y, Yokota R and Kochi M 1997 Spontaneous molecular orientation of polyimides induced by thermal imidization. 3. Component chain orientation in binary polyimide blends *Macromolecules* **30** 5745–52

[24] Ayon A A, Braff R, Lin C C, Sawin H H and Schmidt M A 1999 Characterization of a time multiplexed inductively coupled plasma etcher *J. Electrochem. Soc.* **146** 339–49

[25] Laermer F and Schilp A 1996 Method of anisotropically etching silicon *US Patent Specification* 5501893 (Robert Bosch, GmbH)

[26] Ayon A A, Lin C C, Braff R A, Schmidt M A, Bayt R and Sawin H H 1998 Etching characteristics and profile control in a time multiplexed inductively coupled plasma etcher *Tech. Digest of the 1998 Solid-State Sensor and Actuator Workshop (June 1998)* pp 41–4

[27] Allen M G 1989 Measurement of adhesion and mechanical properties and adhesion of thin films using microfabricated structures *PhD Thesis* Department of Chemical Engineering, Massachusetts Institute of Technology

[28] Allen M G and Senturia S D 1988 Analysis of critical debonding pressures of stressed thin films in the blister test *J. Adhes.* **25** 303–15
[29] Hencky H 1915 Über den Spannungszustand in kreisrunden Platten mit verschwindender Biegungssteifigkeit *Z. Math. Phys.* **63** 311–7
[30] Saif M T A, Alaca B E and Sehitoglu H 1999 Analytical modeling of electrostatic membrane actuator for micro pumps *J. Microelectromech. Syst.* **8** 335–45
[31] Schomburg W K and Goll C 1998 Design optimization of bistable microdiaphragm valves *Sensors Actuators* A **64** 259–64
[32] Beams J W 1959 Mechanical properties of thin films of gold and silver *Structure and Properties of Thin Films* ed C A Neugebauer, J B Newkirk and D A Vermilyea (New York: Wiley)
[33] Maseeh F and Senturia S D 1988 Elastic properties of thin polyimide films *Polyimides: Materials, Chemistry and Characterization, Proc. 3rd Annual Conf. on Polyimides (November 1988)* pp 575–84